JOURNAL OF AIRCRAFT
Vol. 32, No. 4, July–August 1995

Structural Dynamic Loads in Response to Impulsive Excitation

Mordechay Karpel* and Eyal Presente†
Technion–Israel Institute of Technology, Haifa 32000, Israel

The modal approach is used to analyze the dynamic loads on a flexible structure due to local impulsive excitations such as that caused by store ejection from a flight vehicle. First-order, time-domain equations of motion in generalized coordinates are constructed for restrained and free–free structures, without and with unsteady aerodynamic effects. The dynamic loads associated with the structural response are expressed by the mode displacement (MD) and by the summation-of-forces methods. The MD approach is simpler and easier to apply, but requires the inclusion of more modes for obtaining results of acceptable accuracy. A rigorous comparison between the resulting loads shows that the performance of the MD method is especially poor when the excitation is local and impulsive. A dramatic improvement is obtained when the generalized coordinates are based on normal modes calculated with fictitious masses at the excitation points. Fictitious masses are also used to generate artificial load modes that yield simple and efficient expressions for integrated shear forces, bending moments, and torsion moments at various structural sections.

Nomenclature

$[A]$ = state–space system matrix
$[A_1]$, $[A_2]$ = aerodynamic approximation coefficients, Eq. (25)
$[AFC(ik)]$ = complex unsteady aerodynamic force coefficient matrix, Eq. (24)
$[A_s]$ = aerodynamic force coefficient matrix at structural grids, Eq. (24)
$[B]$ = discrete-coordinate damping matrix
$[\bar{B}]$ = generalized damping matrix in aeroelastic model, Eq. (26)
b = reference semichord
$[b]$ = state–space input distribution matrix
$[D]$, $[E]$ = aerodynamic approximation coefficients, Eq. (25)
$\{F(t)\}$ = vector of external forces
$\{F_{ex}\}$ = vector of prescribed excitation forces
$[GB]$ = generalized structural damping matrix
$[GK]$ = generalized structural stiffness matrix
$[GM]$ = generalized structural mass matrix
$[K]$ = discrete-coordinate stiffness matrix
$[\bar{K}]$ = generalized stiffness matrix in aeroelastic model, Eq. (26)
k = reduced frequency, $\omega b/V$
$\{L\}$ = vector of integrated section loads
$[M]$ = discrete-coordinate mass matrix
$[\bar{M}]$ = generalized mass matrix in aeroelastic model, Eq. (26)
n = number of DOF in finite element model
n_m = number of modes taken into account
$[\bar{Q}_{ff}(ik)]$ = approximated generalized aerodynamic force coefficient matrices
$[Q(ik)]$ = generalized aerodynamic force coefficient matrix
q = dynamic pressure
$[R]$ = diagonal aerodynamic lag matrix, Eq. (25)
s = Laplace variable
$[T_{AS}]$, $[T_{CS}]$ = spline transformation matrices, Eq. (24)
$[T_{rb}]$ = rigid-body transformation matrix, Fig. 1
$[T_{\alpha S}]$ = spline transformation matrix, Eq. (24)
t = time
$\{u\}$ = discrete structural displacement vector
V = true airspeed
$\{x\}$ = state vector
y = distance along wingspan
$[\zeta]$ = diagonal modal damping coefficient matrix
$\{\xi\}$ = generalized displacements
$[\phi]$ = matrix of natural modes
$[\chi_n]$ = matrix of vibration modes after fictitious masses are extracted
$[\omega_n]$ = diagonal matrix of natural frequencies mass

Subscripts

a = aerodynamic
f = modes with fictitious masses
i = inboard section
l = load modes
md = mode displacement
n = nominal system
o = outboard section
s = structural
sof = summation of forces

Introduction

THE structures of ground, flight, and space vehicles have to be designed to withstand all the static and dynamic loads they may encounter. The determination of the incremental loads due to time-dependent excitation forces is based on time–domain dynamic response analysis. The net load distribution at a time point during the response is a combination of the prescribed excitation forces, the D'Alembert inertial forces, and other forces that result from the structural response, such as unsteady aerodynamic forces. Integrated loads, such as shear, bending moment, and torsion at a wing section, are calculated during the response analysis. Extreme values of integrated loads are used to define the time points at which load distributions are calculated for stress analysis.

The dynamic response analysis is commonly based on the modal approach[1] in which the structural displacements are represented by a set of low-frequency natural vibration modes (including rigid-body modes), which serve as generalized coordinates. While a typical discrete-coordinate finite element model may have thousands of degrees of freedom (DOF), a typical generalized-coordinate equation of motion has 10–25 DOF (the number of modes taken into account). The number

Received Aug. 22, 1993; revision received Nov. 1, 1994; accepted for publication Nov. 25, 1994.

*Associate Professor, Faculty of Aerospace Engineering. Member AIAA.
†Graduate Student.

of required modes depends on the application, the computer resources, and the required accuracy.

Bisplinghoff et al.[1] described two methods for calculating dynamic loads from the time response in generalized coordinate, the mode displacement (MD) and the mode acceleration (MA) methods. The MD method estimates the external loads from the modal deformations only. The MA method, originally developed by Williams,[2] adds the inertial response loads (calculated from modal accelerations) to the prescribed excitation forces. Williams pointed out the particular advantage of the MA method in calculating loads due to impulsive excitation. An extension of the MA method, which allows other than inertial response-dependent forces, is the summation-of-forces (SOF) method. Applications of the MD and SOF methods in aeroelastic frequency response to aerodynamic excitation are described in Ref. 3. The applications showed that, with eight elastic modes taken into account, both methods were in good agreement. However, with only three elastic modes considered, the SOF method was significantly more accurate than MD.

In cases of time response to local impulsive excitation, such as store ejection or landing, the MD method performs much worse than in Ref. 3. The main reason is that concentrated forces cause local deformations that are not represented in the low-frequency vibration modes. The SOF method is less sensitive to local response effects, but is more difficult to apply, especially when time-domain unsteady aerodynamic effects are involved. The main purposes of this work are to increase the efficiency and accuracy of the two methods in cases of impulsive excitation, and to perform a thorough comparison between them in application to the dynamic response of aeroelastic systems to store ejection.

The impulsive excitation forces during the release of external stores (and in other local-excitation cases) are acting at a small number of DOFs. The improvement of the MD loads is obtained in this work by introducing fictitious masses at the excitation point when the modes are calculated, which causes local deformations in the low-frequency modes, and then removing them in the subsequent dynamic response analysis. The fictitious-mass idea was introduced by Karpel and Newman[4] in the context of modal substructuring. Later applications included repetitive analysis of aircraft with multiple external store configurations,[5] eigenvalue sensitivities of control augmented structures,[6] and flutter analysis with large local structural changes.[7,8]

Unsteady aerodynamic force coefficient matrices are normally available as transcendental functions of the harmonic vibration frequency. The inclusion of unsteady aerodynamic effects in time-domain dynamic response analysis requires the unsteady aerodynamic matrices to be approximated as rational functions of the Laplace variable s. The most common rational approximation method is the term-by-term procedure of Roger.[9] A more general matrix approximation formula is employed by the minimum-state method.[10-12] The minimum-state nonlinear approximation procedure is more complicated than the linear procedure of Roger, but it typically yields a significant reduction in the resulting model size per desired accuracy. The SOF method requires the approximation coefficients to appear not only in the equations of motion, but also in the output equation. It is desired to approximate the output coefficients in a way that does not require additional aerodynamic states. Pototzky and Perry[3] developed such expressions for output parameters in Roger's approximation. The extension of the minimum-state method to include output expressions is a part of the work presented in the following sections.

Structural Equations of Motion

State-space structural equations of motion, in which fictitious-mass modes are used as generalized coordinates, were developed in Refs. 7 and 8 in the context of flutter analysis with large local structural changes. Key equations are repeated in this section for the sake of clarity and completeness. The matrix equation of motion of an n degrees-of-freedom nominal structure is

$$[M]\{\ddot{u}\} + [B]\{\dot{u}\} + [K]\{u\} = \{F(t)\} \tag{1}$$

The common modal approach transforms Eq. (1) to modal coordinates by assuming that $\{u\}$ is a linear combination of a subset of n_m low-frequency natural modes of the nominal structure, where $n_m << n$. The fictitious-mass approach uses normal modes of the fictitious system

$$[M + M_f]\{\ddot{u}\} + [K]\{u\} = \{0\} \tag{2}$$

where $[M_f]$ is a matrix of fictitious masses. The fictitious masses are placed in our application at the m_f DOF in which the impulsive excitation is applied. The values of the fictitious masses should be large enough to cause significant local deformations at the low-frequency modes, but not too large, to avoid numerical ill-conditioning. The $n \times n_m$ matrix of eigenvectors $[\phi_f]$, associated with Eq. (2), satisfies

$$[K][\phi_f] = [M + M_f][\phi_f][\omega_f]^2 \tag{3}$$

where $[\omega_f]^2$ is a diagonal matrix of real non-negative eigenvalues. The diagonal generalized mass and stiffness matrices are

$$[GM_f] = [\phi_f]^T[M + M_f][\phi_f] \tag{4}$$

$$[GK_f] = [\phi_f]^T[K][\phi_f] = [GM_f][\omega_f]^2 \tag{5}$$

The basic assumption of the modal approach, when applied with fictitious-mass modes, is

$$\{u\} = [\phi_f]\{\xi_f\} \tag{6}$$

Substitution of Eq. (6) in Eq. (1), and premultiplication by $[\phi_f]^T$, yield

$$[GM_{fn}]\{\ddot{\xi}_f\} + [GB_f]\{\dot{\xi}_f\} + [GK_f]\{\xi_f\} = [\phi_f]^T\{F(t)\} \tag{7}$$

where

$$[GM_{fn}] = [GM_f] - [\phi_f]^T[M_f][\phi_f]$$

and, when $[B]$ is available, the generalized damping matrix is

$$[GB_f] = [\phi_f]^T[B][\phi_f] \tag{8}$$

The usual case is, however, that $[B]$ is not available and the generalized damping coefficients are chosen using engineering judgment or vibration test results. Since the generalized coordinates in Eq. (7) are not natural modes of the physical system, the assignment of damping coefficients needs special treatment.[7] We first calculate the complete sets of frequencies and eigenvectors $[\omega_n]$ and $[\chi_n]$, associated with the undamped, free equation of motion

$$[GM_{fn}]\{\ddot{\xi}_f\} + [GK_f]\{\xi_f\} = \{0\} \tag{9}$$

where the eigenvectors in $[\chi_n]$ are normalized to yield

$$[GM_n] = [\chi_n]^T[GM_{fn}][\chi_n] = [I] \tag{10}$$

We can now use the coordinate transformation $\{\xi_f\} = [\chi_n]\{\xi_n\}$, to transform Eq. (7) into the uncoupled equation

$$\{\ddot{\xi}_n\} + 2[\zeta_n][\omega_n]\{\dot{\xi}_n\} + [\omega_n]^2\{\xi_n\} = [\chi_n]^T[\phi_f]^T\{F(t)\} \tag{11}$$

where $[\zeta_n]$ is a diagonal matrix of modal damping coefficients associated with the natural frequencies in $[\omega_n]$. The matrix of natural modes associated with $[\omega_n]$ is $[\phi_n] = [\chi_n][\phi_f]$. When the columns of $[\phi_n]$ and the associated frequencies in $[\omega_n]$ are compared to those calculated directly from the nominal finite element model, they appear in two groups. The low-frequency group is practically identical to the directly calculated modes. The modes in the high-frequency group, whose number and nature depend on the number and magnitudes of the fictitious masses, do not represent actual normal modes, but are synthetic modes with relatively large local distortions in the vicinity of the fictitious masses. The coordinate transformation that leads to Eq. (11) may be inconvenient and computationally inefficient, especially when unsteady aerodynamic forces are involved. An alternative way, which is used in the remainder of this article, is to use Eq. (7) with

$$[GB_f] = 2[GM_{fn}][\chi_n][\zeta_n][\omega_n][\chi_n]^T[GM_{fn}] \tag{12}$$

which is "effectively diagonal"[7] because it would yield Eq. (11) if the transformation is performed.

The state–space, first-order form of Eq. (7) is

$$\{\dot{x}\} = [A]\{x\} + [b]\{\bar{u}\} \tag{13}$$

where

$$\{x\} = \begin{Bmatrix} \xi_f \\ \dot{\xi}_f \end{Bmatrix} \qquad [b] = \begin{bmatrix} 0 \\ [GM_{fn}]^{-1}[\phi_f]^T \end{bmatrix} \qquad \{\bar{u}\} = \{F(t)\}$$

$$[A] = \begin{bmatrix} 0 & [I] \\ -[GM_{fn}]^{-1}[GK_f] & -[GM_{fn}]^{-1}[GB_f] \end{bmatrix}$$

Loads Equations

A loading case, for the purpose of structural design, is the vector of the forces that are in equilibrium with the internal elastic forces of the finite element system in Eq. (1):

$$\{F_s(t)\} = [K]\{u(t)\} = \{F(t)\} - [M]\{\ddot{u}(t)\} - [B]\{\dot{u}(t)\} \tag{14}$$

which indicates that, knowing the structural dynamic response from Eq. (13), $\{F_s(t)\}$ can be found by either calculating the elastic forces in the second part of Eq. (14), or by the summation of the excitation, the inertial (D'Alembert), and the damping forces in the right part of Eq. (14). The contribution of the damping forces to the loads distribution is negligible in cases of lightly damped structures. When the modal assumption of Eq. (6) is used with an incomplete set of modes, the two computation methods do not yield identical results. The first one yields the MD loads, via Eqs. (3) and (6):

$$\{F_{md}(t)\} = [K][\phi_f]\{\xi_f(t)\} = [M + M_f][\phi_f][\omega_f]^2\{\xi_f(t)\} \tag{15}$$

The second computation method yields the SOF loads, via Eq. (6) with damping forces neglected:

$$\{F_{sof}(t)\} = \{F(t)\} - [M][\phi_f]\{\ddot{\xi}_f(t)\} \tag{16}$$

Detailed loading cases for stress analysis are calculated only at extreme conditions. The time points at which extreme conditions occur are defined by criticality criteria that are based on selected integrated loads, such as shear force and bending moments at a wing section. Section loads are calculated by integrating the distributed loads over the structure, between the section and a free end, with multiplication by the appropriate arms for section moments. A matrix $[\phi_l]$ of kinematic "load modes" is defined for the numerical integration to obtain the MD integrated loads

$$\{L_{md}(t)\} = [\phi_l]^T[M + M_f][\phi_f][\omega_f]^2\{\xi_f(t)\} \tag{17}$$

and the SOF integrated loads

$$\{L_{sof}(t)\} = [\phi_l]^T\{F(t)\} - [\phi_l]^T[M][\phi_f]\{\ddot{\xi}_f(t)\} \tag{18}$$

The shape of a load mode in $[\phi_l]$ is that of a broken structure with rigid-body segments. The definition of $[\phi_l]$ and the matrix operations to obtain the load coefficient matrices, here and in the aeroelastic models below, might require extensive postprocessing work because they are not standard features of common finite element codes such as MSC/NASTRAN.[13] A new technique, which simplifies the matrix operations and facilitates a convenient way to define the load modes, is presented here. The technique extends the way control modes are treated in Ref. 14 to allow an overdetermined connection between the structural segments. Fictitious-mass concepts are used with very large masses to obtain the rigid-body load modes from the same natural mode analysis that generates the structural modes, without affecting them.

The following changes, described in NASTRAN's terminology, are introduced to the finite element model in order to deal with integrated loads at a certain section (see Fig. 1).

1) The section grid points are triplicated to form three collocated identical groups that define an inboard, a middle, and an outboard section. The respective displacement vectors are $\{u_i\}$, $\{u_m\}$, and $\{u_o\}$.

2) The inboard points must be connected to the inboard structural elements only, and the outboard points to the outboard elements.

3) A new grid point with n_l degrees-of-freedom $\{u_l\}$, which represent the relative motion, where $n_l \leq 6$ is the number of the desired section load modes, is added at a reference point in the section. The output coordinate system associated with this grid point defines the reference axes for bending and torsion.

4) The middle-section coordinates are connected with rigid elements (RBE2 in NASTRAN) to the reference point, which defines the constraints $\{u_m\} = [T_{rb}]\{u_l\}$, where $[T_{rb}]$ is a rigid-body transformation and $\{u_m\}$ becomes dependent.

5) Another set of constraints defines $\{u_o\} = \{u_i\} + \{u_m\}$ [by multi-point constraint (MPC) cards in NASTRAN] such that $\{u_o\}$ becomes a dependent displacement set that satisfies

$$\{u_o\} = \{u_i\} + [T_{rb}]\{u_l\} \tag{19}$$

6) The coordinates $\{u_l\}$ are loaded with a diagonal mass matrix $[M_l]$ whose elements are very large (several orders of magnitude larger than other mass elements, including the fictitious masses in $[M_f]$).

The modified model has n_l more DOFs than the original one. Normal modes analysis of the modified model produces two sets of modes. The n_l load modes appear as rigid-body modes $[\phi_l]$ that can be normalized such that the partition associated with the relative motion $\{u_l\}$ is a unit matrix. Since

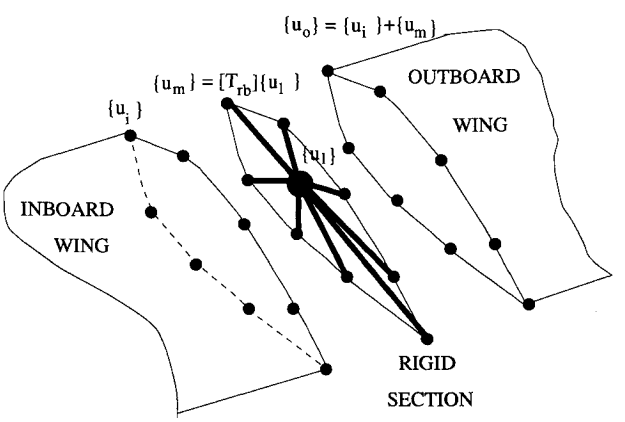

Fig. 1 Modeling of a section at which integrated loads are requested.

$\{u_l\}$ is loaded with very large masses, these modes consist of the added relative motion only, whereas the inboard segment does not move and the outboard segment is kinematically defined by the relative motion. As argued below, the other modes are practically identical to the original modes $[\phi_f]$, expanded to include the small modal deflections $[\phi_{fl}]$ associated with $\{u_l\}$. Since the load modes and the structural modes are extracted in the same eigensolution, they are orthogonal, which implies

$$\begin{bmatrix} \phi_l \\ I \end{bmatrix}^T \begin{bmatrix} M + M_f & 0 \\ 0 & M_l \end{bmatrix} \begin{bmatrix} \phi_f \\ \phi_{fl} \end{bmatrix} = [0] \tag{20}$$

which yields

$$[\phi_l]^T[M + M_f][\phi_f] = -[M_l][\phi_{fl}] \tag{21}$$

Since the diagonal terms in $[M_l]$ are very large, the terms in $[\phi_{fl}]$ are very small, which implies that the changes introduced to generate the load modes have a negligible effect on the structural modes. Substitution of Eq. (21) into Eqs. (17) and (18) yields

$$\{L_{md}(t)\} = -[M_l][\phi_{fl}][\omega_f]^2\{\xi_f(t)\} \tag{22}$$

$$\{L_{sof}(t)\} = [\phi_l]^T\{F(t)\} + ([M_l][\phi_{fl}] + [\phi_l]^T[M_f][\phi_f])\{\ddot{\xi}_f(t)\} \tag{23}$$

The advantage of the modified MD coefficients in Eq. (22), over the original ones in Eq. (17), is very clear. The need for explicit definition of $[\phi_l]$ is eliminated, and the computations now involve only the few large masses, the modal deflections at the large-mass coordinates, and the elastic natural frequencies, compared to the large-order mass and mode matrices in Eq. (17). The SOF coefficients of $\{\ddot{\xi}_f\}$ in Eq. (23) are also considerably easier to compute compared to those in Eq. (18) because there are only a few nonzero terms in $[M_f]$ as well. Still, $\{L_{sof}\}$ is a function of the excitation forces and all the states, via $\{\ddot{\xi}_f\}$ in Eq. (13), while $\{L_{md}\}$ is a function of the displacements only. The computational advantage of the MD method over SOF is even bigger when the external forces are affected by the structural motion, which is the case when unsteady aerodynamic forces are involved.

Aeroelastic Equations

The structural dynamic response of a flying vehicle involves unsteady aerodynamic forces generated by surface motion. Common unsteady aerodynamic computation methods, such as the doublet lattice method,[15] can be used to calculate the complex unsteady aerodynamic force coefficient (AFC) matrices due to modal harmonic oscillations for various reduced frequencies $k = \omega b/V$. The aerodynamic model is based on panels, each having a center of pressure point A and a downwash control point C. The self-excitation frequency-domain aerodynamic forces acting on the vehicle in the structural grid are

$$\{F_a(ik)\} = -q[A_s(ik)]\{\xi_f(ik)\} \tag{24}$$

where

$$[A_s(ik)] = [T_{AS}]^T[AFC(ik)][(ik/b)[T_{CS}] + [T_{\alpha S}]][\phi_f]$$

where $[T_{AS}]$, $[T_{CS}]$, and $[T_{\alpha S}]$ are spline transformation matrices from deflections at the structural points to normal deflections at points A and C, and angle-of-attack rotations at points C, respectively. To facilitate the calculation of SOF loads with standard aerodynamic codes, the load modes $[\phi_l]$ are included, with the normal modes $[\phi_f]$, in the set of modes for which the generalized aerodynamic force (GAF) matrices, $[Q_{ff}(ik)] = [\phi_f]^T[A_s(ik)]$ and $[Q_{lf}(ik)] = [\phi_l]^T[A_s(ik)]$, are calculated.

Time-domain modeling requires the GAFs to be approximated by rational interpolation functions in the Laplace s domain. It is desired to include the coefficients associated with the load modes in the approximation without affecting the size of the resulting state-space model. The application of Roger's approximation[9] to dynamic loads analysis required the development of special terms for the load matrices.[3] The aerodynamic approximations in this work are performed by the minimum-state (MS) method,[10-12] which is somewhat more complicated, but typically yields a considerably lower number of aerodynamic states. Due to its generality, the MS method is applicable to dynamic loads with only a minor modification. The approximation function, constrained to exactly match steady aerodynamics, is

$$\begin{bmatrix} \bar{Q}_{ff} \\ \bar{Q}_{lf} \end{bmatrix} = \begin{bmatrix} Q_{ff}(0) \\ Q_{lf}(0) \end{bmatrix} + \begin{bmatrix} A_{1_f} \\ A_{1_l} \end{bmatrix} \bar{s} + \begin{bmatrix} A_{2_f} \\ A_{2_l} \end{bmatrix} \bar{s}^2 + \begin{bmatrix} D_f \\ D_l \end{bmatrix} (\bar{s}[I] - [R])^{-1}[E]\bar{s} \tag{25}$$

where $\bar{s} = sb/V$. The user defines the $m \times m$ diagonal aerodynamic lag matrix $[R]$ and two additional approximation constraints (for each term), which define $[A_{1_f}]$, $[A_{1_l}]$, $[A_{2_f}]$, and $[A_{2_l}]$ as functions of the other matrix coefficients and the tabulated data. The $[D_f]$ and $[E]$ real coefficient matrices are calculated by an iterative nonlinear least-square procedure that fits the tabulated data matrices.[11] The modification introduced in this work is that the resulting $[E]$ is used to calculate $[D_l]$ with no iterations. In this way $[D_f]$ and $[E]$ are not affected by the presence of $[\bar{Q}_{lf}]$ in the approximation, which implies that the equations of motion are not affected by the number and type of output loads equations.

A full development of the state-space aeroelastic equations of motion with aerodynamic control and gust excitations is given in Ref. 16. The equation of motion of the aeroelastic system with prescribed external excitation is

$$\{\dot{x}\} = [A]\{x\} + [b]\{\bar{u}\} \tag{26}$$

where

$$\{x\} = \begin{Bmatrix} \xi_f \\ \dot{\xi}_f \\ x_a \end{Bmatrix} \qquad [b] = \begin{bmatrix} 0 \\ [GM_{fn}]^{-1}[\phi_f]^T \\ 0 \end{bmatrix} \qquad \{\bar{u}\} = \{F_{ex}(t)\}$$

$$[A] = \begin{bmatrix} 0 & [I] & 0 \\ -[\bar{M}]^{-1}[\bar{K}] & -[\bar{M}]^{-1}[\bar{B}] & -q[\bar{M}]^{-1}[D_f] \\ 0 & [E] & (V/b)[R] \end{bmatrix}$$

$$[\bar{M}] = [GM_{fn}] + (qb^2/V^2)[A_{2_f}] \qquad [\bar{K}] = [GK_f] + q[Q_{ff}(0)]$$

$$[\bar{B}] = [GB_f] + (qb/V)[A_{1_f}]$$

where $\{x_a\}$ is a vector of m aerodynamic states. The state response $\{x(t)\}$ to initial conditions and prescribed excitation forces can be solved for by standard numerical time-simulation routines. Static (steady-state) response to step excitation can be obtained from the second row partition of Eq. (26) with $\{\ddot{\xi}_f\} = \{\dot{\xi}_f\} = \{x_a\} = (0)$, which yields

$$\{\xi_f\} = ([GK_f] + q[Q_{ff}(0)])^{-1}[\phi_f]^T\{F_{ex}\} \tag{27}$$

where it is assumed that q is smaller than the dynamic pressure of aeroelastic divergence.

The aerodynamic contribution to the SOF loads is calculated from the state response of Eq. (26). The section loads in Eq. (23) are supplemented by the aerodynamic terms

$$\{L_a\} = -q[Q_{lf}(0)]\{\xi_f\} - (qb/V)[A_{1_f}]\{\dot{\xi}_f\} - (qb^2/V^2)[A_{2_f}]\{\ddot{\xi}_f\} - q[D_l]\{x_a\} \quad (28)$$

When complete SOF load distributions [Eq. (16)] are of interest, the bottom partition of the aerodynamic approximation in Eq. (25) can be expanded to include the approximation of $[A_s(ik)]$ of Eq. (24). Equation (16) can then be supplemented by Eq. (28) with the associated coefficient matrices.

Numerical Example

The numerical example is based on the high aspect ratio wing model adopted and modified from Ref. 17. A top view of the NASTRAN structural model, which consists of about 300 grid points, is shown in Fig. 2. The wing semispan is 12 m and its total weight is 1700 kg. The purpose of the numerical example is to demonstrate the enhanced MD and SOF methods, especially when applied to aeroelastic systems under local impulsive excitation. The dynamic loads are due to the response (from zero initial conditions) to a step excitation force of 1 N, applied near the middle of the wing section at $y = 7.76$ m. This case represents incremental loads due to the release of external stores from a flight vehicle, simplified for the purpose of clarity.

We start with the case of a cantilevered wing with no aerodynamics. Load modes were generated for the calculation of the integrated shear force, bending moment, and torsion moment at 17 sections along the wingspan, which required the addition of 17 grid points, each having DOFs in the z, θ_x, and θ_y directions. The 51 added DOFs, $\{u_l\}$ in Eq. (19), were loaded by the mass matrix $[M_l] = 10^{11}[I]$ where the mass terms associated with θ_x and θ_y are mass moments of inertia. The 16 grid points at each section were triplicated while the new points were constrained to the original ones and to $\{u_l\}$ by Eq. (19). As expected, the introduction of the section-load points and the associated large masses added 51 "broken" rigid-body modes with negligible effects on the elastic frequencies and modes.

The required modal data was first generated without fictitious masses at the excitation point, $[M_f] = [0]$. The first demonstration is of the resulting static (steady-state) loads. The associated SOF shear forces, bending moments and torsion moments are 1, $7.76 - y$, and $-2.35 + 0.34y$, respectively, inboard of section $y = 7.76$ m, and 0 outboard of this section. Since the convergence rates and accuracy levels for the torsion moments throughout the numerical example are similar to those of the bending moments, and since the torsion moments are relatively small in our high aspect ratio wing, we found it sufficient to present and discuss the shear forces and bending moments only. The variations of integrated shear and bending moment along the wingspan, calculated by the MD method with various numbers of wing vibration modes, are shown in Fig. 3. This case demonstrates the main problem

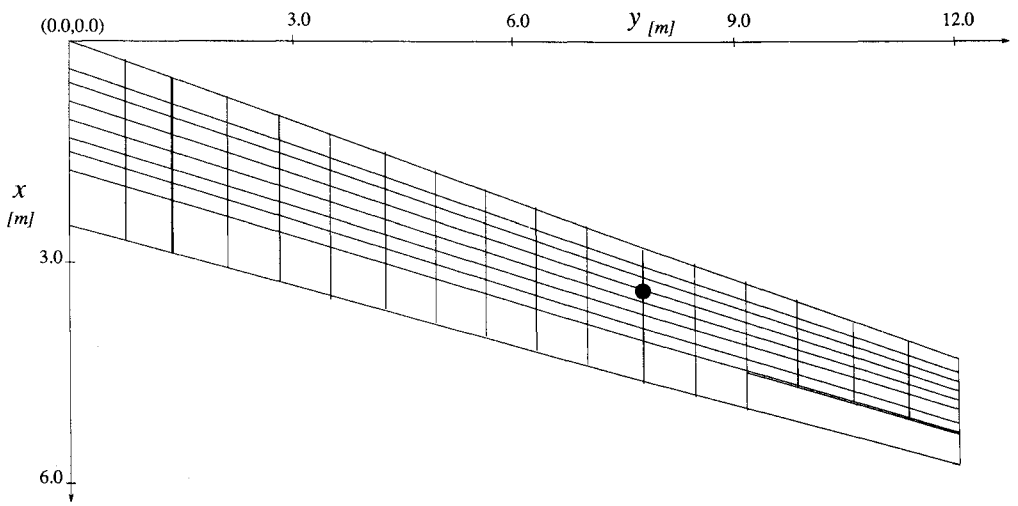

Fig. 2 Top view of the structural wing model.

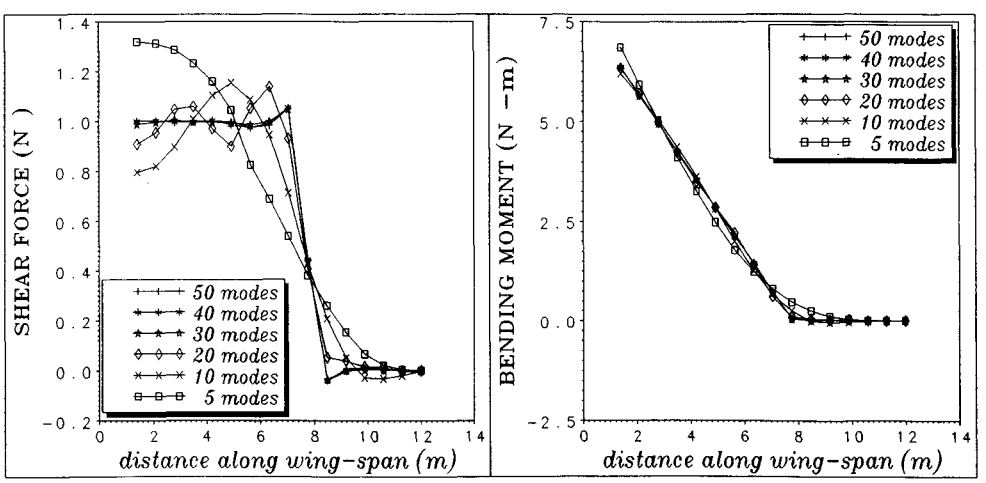

Fig. 3 Mode-displacement shear forces and bending moments along the wingspan, cantilevered, static, no aerodynamics, $M_f = 0$.

Table 1 Natural frequencies (Hz) from nominal and fictitious-mass models

Mode no.	Nominal frequency	n_m = 5	10	15	20	Largest error, %
1	3.138	3.142	3.138	3.138	3.137	0.147
2	8.717	8.717	8.717	8.717	8.717	0.000
3	11.077	11.144	11.081	11.078	11.077	0.601
4	11.679	(12.262)	11.693	11.680	11.679	0.120
5	12.898	12.898	12.898	12.898	12.898	0.000
6	22.929	—	22.930	22.929	22.929	0.002
7	24.935	—	25.056	24.945	24.937	0.484
8	36.156	—	36.160	36.156	36.156	0.010
9	39.841	—	40.334	39.882	39.852	1.236
10	42.794	—	(53.165)	42.896	42.822	0.238
11	52.314	—	—	52.314	52.314	0.000
12	52.351	—	—	52.351	52.351	0.000
13	56.508	—	—	56.926	56.597	0.738
14	62.509	—	—	62.507	62.506	0.005
15	69.646	—	—	(102.235)	69.647	0.001
16	71.595	—	—	—	71.661	0.091
17	73.085	—	—	—	73.117	0.044
18	85.513	—	—	—	86.129	0.720
19	96.783	—	—	—	98.071	1.331
20	98.463	—	—	—	(125.206)	—

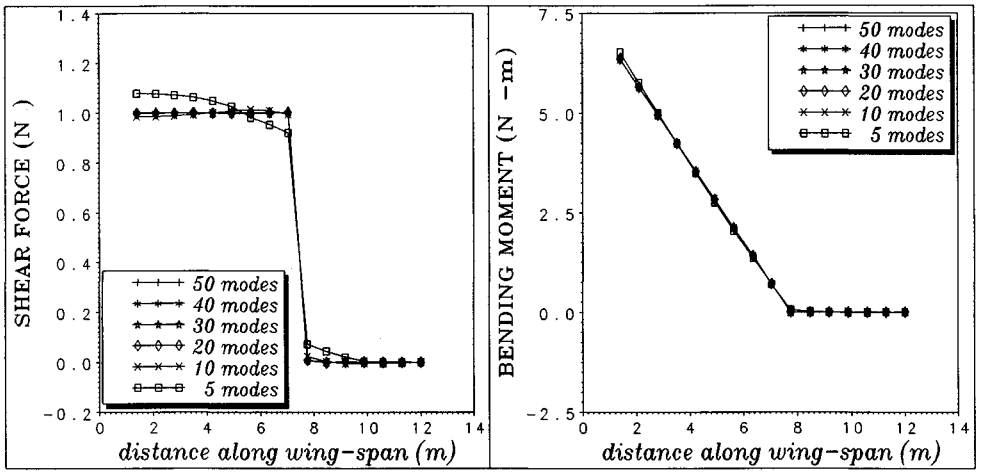

Fig. 4 Mode-displacement shear forces and bending moments along the wingspan, cantilevered, static, no aerodynamics, M_f = 2000 kg.

in using the MD method to estimate loads due to concentrated forces. More than 20 modes are required to obtain reasonable shear forces far from the excitation point. Even 50 modes are not sufficient to obtain high-accuracy shear forces near the excitation point. The bending moments are more accurate because they are continuous at the excitation point. The same MD integrated loads, this time based on modes calculated with a single additional fictitious-mass term of 2000 kg loading the excitation point in z direction, are shown in Fig. 4. With 10 modes we now get error levels of less than 2% over the entire wing. The dramatic improvement is caused by the fact that the low-frequency modes now contain significant local distortions near the excitation point, which allows sharp gradients in the resulting load distribution. The MD bending moments errors are now less than 2%, even with five modes.

The natural frequencies $[\omega_n]$, obtained by calculating the fictitious-mass modal properties and then removing the fictitious mass using Eqs. (7) and (9), are compared in Table 1 to the natural frequencies of the nominal structure. One frequency in each case, usually the last one, is related to a synthetic local-deformation mode. The synthetic frequency in the five-mode case is the fourth one, whereas the fifth one relates to in-plane motion that is not affected by the fictitious mass. The other frequencies in all the cases are practically identical to the nominal ones.

As shown in previous applications,[4,5,8] it is easy to choose an adequate size for the fictitious mass. It is only required that this mass be considerably larger than other masses in the model, such as M_f = 2000 kg compared with the total wing mass of 1700 kg in our case, but not large enough to cause numerical ill-conditioning. Application of excitation forces at different locations simultaneously requires several fictitious masses, which yields more local-deformation modes and requires more modes to be considered. Hence, the fictitious-mass approach is efficient only with a limited number of large fictitious masses.

The maximum shear forces along the wingspan, calculated by the MD method during the dynamic response to the step force, are shown in Fig. 5 for the nominal and fictitious-mass cases. The modal damping coefficients $[\zeta_n]$ in Eq. (12) are 0.01 for all modes, except for the one associated with the highest frequency of the fictitious-mass case that is set to 0.07 to avoid unrealistically excessive vibrations of the synthetic mode. Here again, fictitious-mass MD loads are considerably more accurate than the nominal ones, especially near the excitation point. The SOF shear forces (not shown) are practically identical to the MD shear in the fictitious-mass case with 20 modes and more. The comparison of the nominal-case part of Fig. 5 with the static shear forces in Fig. 3 indicates that the MD errors are mainly in the static part of the solution.

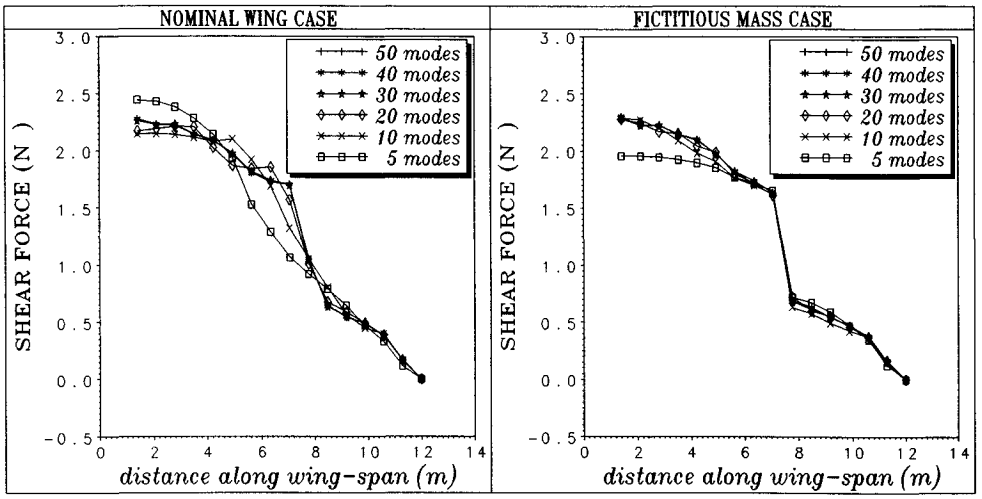

Fig. 5 Mode-displacement maximum dynamic shear forces along the wingspan, cantilevered, no aerodynamics, $M_f = 0$ (nominal case) and $M_f = 2000$ kg.

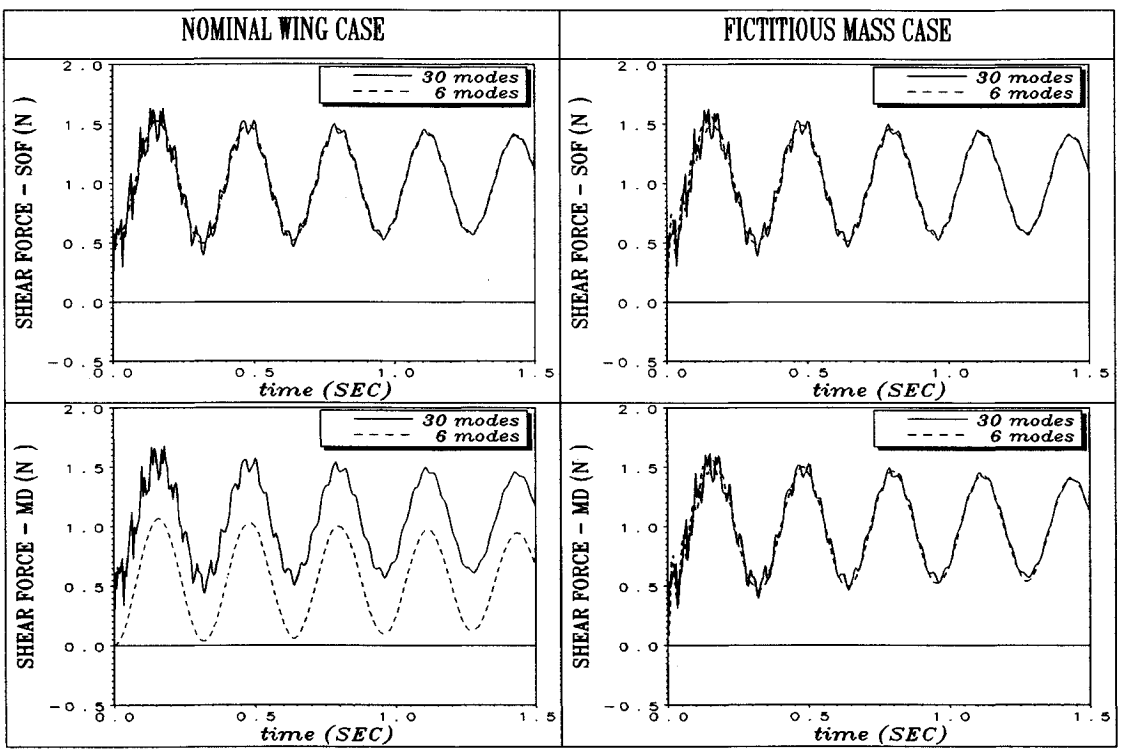

Fig. 6 MD and SOF dynamic shear forces vs time, cantilevered, no aerodynamics.

The dynamic (inertial) part of the loads is distributed quite evenly, and hence, estimated well by the nominal modes. This point is also demonstrated in Fig. 6, which shows time histories of the shear force at $y = 7.05$ m (0.71 m inboard of the excitation point). It can be observed that the main difference between the 6-mode and the 30-mode nominal MD cases is a steady shift. This gap is closed by the introduction of the fictitious mass. It can also be observed that the introduction of the fictitious mass does not have a significant effect on the SOF loads.

The rest of the numerical example takes into account the aerodynamic forces. Frequency-domain unsteady GAF matrices were calculated by the doublet lattice method, Mach 0.7, for the 12 reduced frequencies $k = 0., 0.01, 0.04, 0.07, 0.1, 0.35, 0.55, 0.75, 1.0, 1.5, 2.5$, and 4.0, with the reference semichord $b = 0.5$ m. Two aerodynamic approximations, fully unsteady and quasisteady, were performed to define the GAF matrix as rational functions of the Laplace variable. The fully unsteady approximation of Eq. (25) was generated by the MIST code[12] with 10 aerodynamic lag terms, which yields 10 aerodynamic states. The quasisteady approximation was performed by setting $[A_{1_f}] = \text{Im}[Q_{1_f}(0.01)]/0.01$, $[A_{1_l}] = \text{Im}[Q_{1_l}(0.01)]/0.01$, and $[A_{2_l}] = [A_{2_l}] = [0]$, and dropping the aerodynamic lag term (the last one) in Eq. (25), which yields an equation of motion (26) with no aerodynamic states.

Convergence plots of the maximum shear force at $y = 7.05$ m, calculated by the various methods at dynamic pressure of $q = 15{,}680$ N/m^2, are shown in Fig. 7. The quasisteady and the unsteady plots are very similar to each other with the converged unsteady values being about 2% larger than the quasisteady values. The effect of including aerodynamic lag terms is expected to be more significant near the flutter boundary, which is far from the calculated response point. A comparison with the fictitious-mass loads at this section in Fig. 5 shows that the aerodynamic forces reduce the maximum dynamic loads by about 15%. As before, the fictitious mass

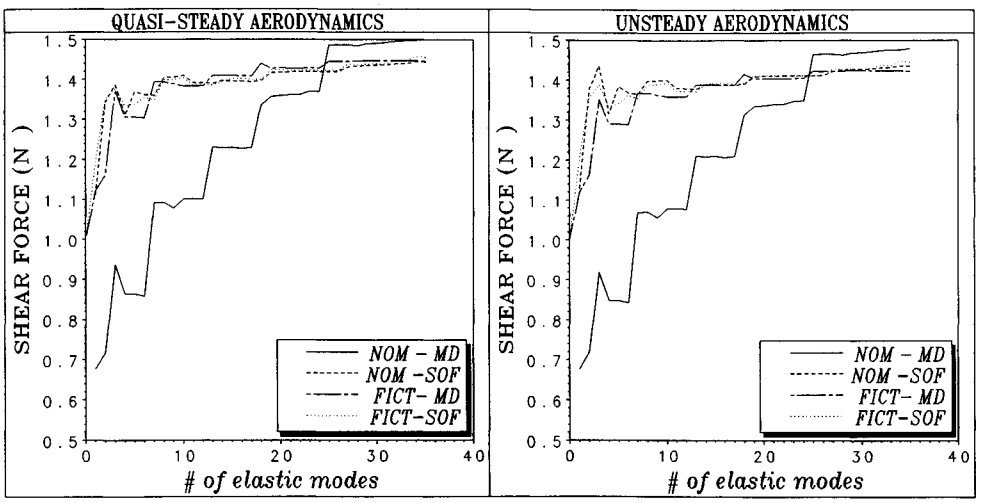

Fig. 7 Maximum shear forces at $y = 7.05$ m vs number of elastic modes, cantilevered, quasisteady, and unsteady aerodynamics.

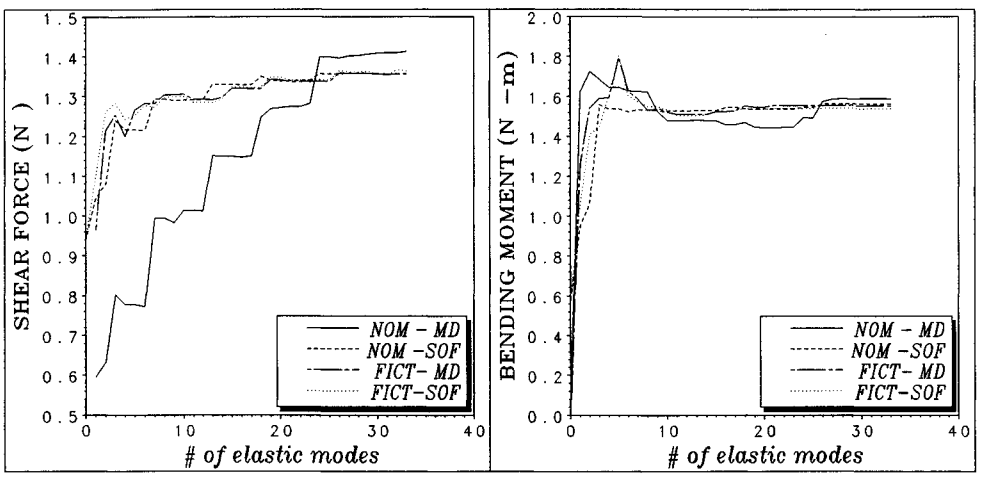

Fig. 8 Maximum shear forces and bending moments at $y = 7.05$ m vs number of elastic modes, free–free (symmetric), quasisteady aerodynamics.

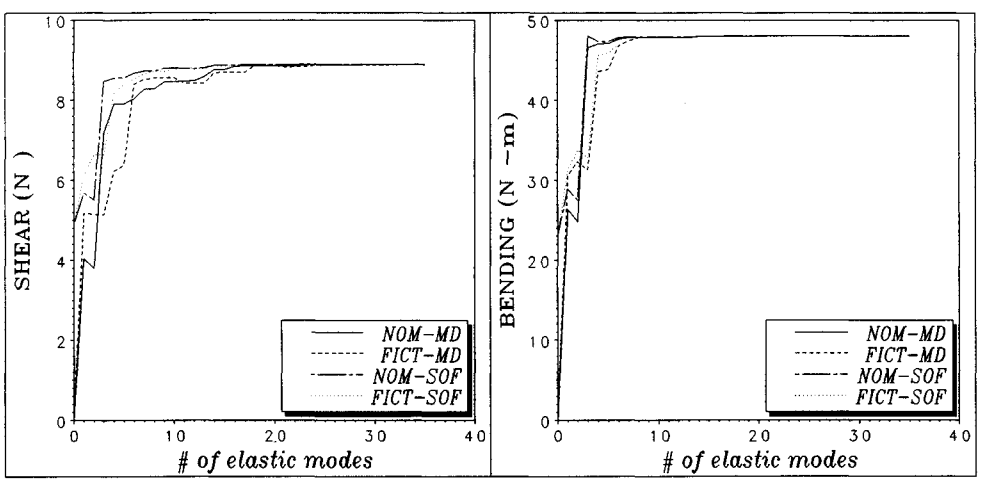

Fig. 9 Maximum wing–root shear force and bending moment due to step angle of attack.

has a dramatic effect on the accuracy of the MD loads, and it does not affect the accuracy of the SOF loads.

Dynamic loads were also calculated for the free–free aircraft with symmetric boundary conditions. The wing model was extended in this case to include a rigid fuselage whose weight was about five times that of the wing. The aerodynamic loads on the added part were ignored. Convergence plots of the maximum shear force and bending moment at $y = 7.05$ m, calculated with quasisteady aerodynamics with the number of elastic modes, are shown in Fig. 8. A comparison with Fig. 7 shows that the inclusion of rigid-body motion reduces the maximum shear loads by about 7% (due to inertia relief effects). The convergence behavior of the free–free case are similar to those of the cantilevered cases.

To complete the investigation, we calculated dynamic MD and SOF loads due to the well-distributed excitation caused

by a step angle of attack. Maximum wing-root shear forces and bending moments vs number of modes are shown in Fig. 9. The fictitious mass in the "FICT" cases is located in the same point as in the previous examples, even though there is no excitation now at this point. The MD loads here are considerably more accurate than in the local excitation cases. It can be observed that, with a small number of modes, the SOF method still yields more accurate results than the MD method, and that the presence of the fictitious mass does not affect the results significantly. With 8 modes and more for the moment case, and with 15 modes and more for the shear-force case, all the methods converge to practically the same results.

Conclusions

Load distributions and integrated section loads during the dynamic response of structures can be calculated from the outputs of linear time-invariant generalized-coordinate state-space equations of motion by either the MD or SOF methods. While the MD loads are functions of the time history of the generalized displacements only, SOF loads are functions of the time history of all the states and the excitation forces. However, in cases of impulsive local excitation, the MD loads are shown to require a relatively large number of natural vibration modes to be taken into account. This problem is solved, for cases with a small number of excitation locations, by using fictitious masses at the excitation points when the modes are calculated. With this method, the convergence of the MD loads with the number of modes is similar to that of the SOF loads. A numerical example of a single concentrated force acting on a high aspect ratio wing demonstrates that the modified MD and the SOF methods with 10 elastic modes yield error levels of less than 2%. Unsteady aerodynamic effects are introduced by the minimum-state modeling method that added 10 aerodynamic states to numerical applications with up to 70 structural states. The minimum-state procedure is modified to allow the inclusion of unsteady effects in the SOF output equations without increasing the model size. The aerodynamic effects on the response to store ejection are shown to be significant (about 15% reduction). However, comparisons of dynamic loads with fully unsteady aerodynamics and with quasisteady aerodynamics (which do not require aerodynamic states), shows very small differences between them (less than 2%). The dynamic loads on the free-free case were about 7% smaller than those of the cantilevered wing case, due to rigid-body inertia relief effects. Well-distributed excitation cases were not affected significantly by the presence of fictitious masses. SOF loads were more accurate in these cases only when less than 15 modes were taken into account. With more modes and with fictitious masses at points of local excitation, the simpler MD method is preferable.

Acknowledgment

The work presented in this article was partially supported by NASA Grant NAGW-1708. This support is gratefully acknowledged.

References

[1]Bisplinghoff, R. L., Ashley, H., and Halfman, R. L., *Aeroelasticity*, Addison-Wesley, Reading, MA, 1955.

[2]Williams, D., "Dynamic Loads in Aeroplanes Under Given Impulsive Loads with Particular Reference to Landing and Gust Loads on a Large Flying Boat," British Royal Aircraft Establishment Repts. 3309 and 3316, 1945.

[3]Pototzky, A. S., and Perry, B., III, "New and Existing Techniques for Dynamic Loads Analyses of Flexible Airplanes," *Journal of Aircraft*, Vol. 23, No. 4, 1986, pp. 340-347.

[4]Karpel, M., and Newman, M., "Accelerated Convergence for Vibration Modes Using the Substructure Coupling Method and Fictitious Coupling Masses," *Israel Journal of Technology*, Vol. 13, Feb. 1975, pp. 55-62.

[5]Karpel, M., "Efficient Vibration Mode Analysis of Aircraft with Multiple External Store Configurations," *Journal of Aircraft*, Vol. 25, No. 8, 1988, pp. 747-751.

[6]Livne, E., "Accurate Calculation of Control Augmented Structural Eigenvalue Sensitivities Using Reduced Order Models," *AIAA Journal*, Vol. 27, No. 7, 1989, pp. 947-954.

[7]Karpel, M., and Wieseman, C. D., "Modal Coordinates for Aeroelastic Analysis with Large Local Structural Variations," *Journal of Aircraft*, Vol. 31, No. 2, 1994, pp. 396-403.

[8]Karpel, M., and Wieseman, C. D., "Time Simulation of Flutter with Large Stiffness Changes," *Journal of Aircraft*, Vol. 31, No. 2, 1994, pp. 404-410.

[9]Roger, K. L., "Airplane Math Modeling Methods for Active Control Design. Structural Aspects of Active Controls," AGARD CP-228, 1977, pp. 4.1-4.11.

[10]Karpel, M., "Design for Active Flutter Suppression and Gust Alleviation Using State-Space Aeroelastic Modeling," *Journal of Aircraft*, Vol. 19, No. 3, 1982, pp. 221-227.

[11]Karpel, M., "Time-Domain Aeroservoelastic Modeling Using Weighted Unsteady Aerodynamic Forces," *Journal of Guidance, Control, and Dynamics*, Vol. 13, No. 1, 1990, pp. 30-37.

[12]Karpel, M., and Hoadley, S. T., "Physically Weighted Approximations of Unsteady Aerodynamic Forces Using the Minimum-State Method," NASA TP-3025, March 1991.

[13]Gockel, M. A. (ed.), *MSC/NASTRAN Handbook for Dynamic Analysis*, MacNeal Schwendler Corp., Los Angeles, CA, 1983.

[14]Karpel, M., "Multidisciplinary Optimization of Aeroservoelastic Systems Using Reduced-Size Models," *Journal of Aircraft*, Vol. 29, No. 5, 1992, pp. 939-946.

[15]Albano, E., and Rodden, W. P., "Doublet-Lattice Method for Calculating Lifting Disturbances of Oscillating Surfaces in Subsonic Flow," *AIAA Journal*, Vol. 2, No. 2, 1969, pp. 279-285.

[16]Karpel, M., "Size-Reduction Techniques for the Determination of Efficient Aeroservoelastic Models," *Control and Dynamic Systems—Advances in Theory and Applications*, Vol. 54, Academic, San Diego, CA, 1992, pp. 263-295.

[17]Bindolino, G., Lanz, M., Mantegazza, P., and Ricci, S., "Integrated Structural Optimization in the Preliminary Aircraft Design," *Proceedings of the 17th Congress of the International Council of the Aeronautical Sciences* (Stockholm, Sweden), 1990, pp. 1366-1378.